Journal of Magnetic Resonance **147,** 78–88 (2000)
doi:10.1006/jmre.2000.2162, available online at http://www.idealibrary.com on IDEAL®

Multiple-Time Correlation Functions in Spin-3/2 Solid-State NMR Spectroscopy

Roland Böhmer

Institut für Physikalische Chemie, Johannes Gutenberg-Universität, 55099 Mainz, Germany

Received January 4, 2000; revised May 25, 2000

Stimulated echo spectroscopy of nonselectively excitable $I = 3/2$ nuclei offers new perspectives for the investigation of ultraslow motions predominantly in inorganic solids and solid-like materials. Conditions for the generation of pure, quadrupole modulated multipolar spin orders and for the detection of two- and four-time correlation functions are discussed. The case of spins $I > 3/2$ is also briefly considered. © 2000 Academic Press

Key Words: **multipolar spin order; phase cycles; quadrupolar nuclei; stimulated spin echoes.**

1. INTRODUCTION

A number of multidimensional NMR techniques for the investigation of exchange phenomena in solids and solid-like materials rely on the application of stimulated echo spectroscopy. Many of these methods involve deuterons or carbons as nuclear probes (*1*). Apart from ^{2}H and ^{13}C also ^{15}N and ^{31}P, i.e., other nuclei with spin $I = 1/2$ or 1, were employed and yielded detailed insights into the dynamics, predominantly of organic materials. For NMR studies of inorganic solids it is often more convenient to utilize quadrupolar nuclei with $I > 1$. Techniques for the elucidation of *structural* properties of solid materials have greatly benefited from fast sample rotation (*2*). However, *dynamical* aspects, via $I > 1$ nuclei, are almost exclusively studied using more conventional approaches such as lineshape analysis and spin-relaxation methods (*3, 4*). This holds true in particular for many solids for which the NMR spectra have to be treated in second-order perturbation theory (*5*). For solid materials in which only first-order quadrupolar perturbations are relevant, one may apply stimulated echo techniques for a detection of translational motions directly in the ultraslow regime. The first such applications employing spin-3/2 nuclei in solids include a study of the ^{9}Be dynamics in metallic glasses (*6*) and the investigation of the ^{7}Li jump processes in crystalline ion conductors (*7*). In both experiments the Jeener–Broekaert echo was recorded as a function of the mixing time, t_m. Echo attenuation then arises predominantly if the probe nuclei, prior and subsequent to t_m, are subject to different electrical field gradients (EFGs) and hence quadrupolar frequencies. The quadrupolar spin order which is stable during t_m thus serves as a state which allows the information to be stored on the quadrupolar frequency ω_Q experienced by a probe nucleus prior to t_m. Then, by comparing it with the quadrupolar frequency after the mixing interval, a two-point time-correlation function can be monitored by recording Jeener–Broekaert echo amplitudes for variable t_m.

Since the work of Jaccard *et al.* (*8*), multipolar spin orders are also exploited in the study of spin-3/2 nuclei in liquid-like environments. Most applications in this area are concerned with the detection of sodium ions in partially ordered, biologically relevant samples. Here one often aims at separating a fully averaged NMR line typically originating from probe nuclei in isotropic solutions from a line which exhibits a residual quadrupolar coupling. This separation can be accomplished using multiple quantum (MQ) selection schemes. Thus the spin states generated during t_m are typically employed to filter out unwanted coherences (*9–11*). In liquid-like environments Jeener–Broekaert-type experiments are usually carried out with variable evolution times in order to yield two-dimensional spectra.

In contrast, in the present article constant evolution but variable mixing times will be considered. This is because we wish to explore to what extent the deuteron (and carbon) stimulated echo experiments, which for organic materials have been very successful in unraveling the dynamics taking place during the mixing time, can be adapted to study inorganic solids using suitable nuclear probes. In the stimulated ($I \leq 1$) echo spectroscopy of solid-like materials it has recently been found quite useful to correlate the NMR frequencies for more than two points in time (*12*). So far, corresponding experiments have been carried out for a variety of amorphous substances using ^{2}H and ^{13}C NMR. Here the NMR frequency typically reflects the orientation of the chemical bonds in which the probe nuclei are located. A well-known application is to use, e.g., the Jeener–Broekaert sequence as a low-pass filter (*13*). This is possible because only the magnetization of those nuclei for which the interaction tensors have not reoriented during the mixing time contributes to the echo significantly. These probes consequently belong to "slow" molecules. Thus, the Jeener–Broekaert and related sequences enable one to select slow subensembles out of broad distributions of reorientational correlation times; the latter are a hallmark of glass-forming ma-

1090-7807/00 $35.00
Copyright © 2000 by Academic Press
All rights of reproduction in any form reserved.

terials (*14*). The low-pass filtered components can be investigated using subsequent multiple-pulse sequences resulting in the generation of a four-point correlation function, e.g., in order to check the efficiency of low-pass filtering. This efficiency in turn can yield information on the intrinsic exponentiality of the reorientational correlation functions (*13*).

By correlating the NMR frequencies at four points in time in a different manner, a related experimental approach allows one to unravel the time scale on which an effective slow ↔ fast exchange might take place. This enables one to find out how long it takes for an amorphous material to "forget" low-pass filtering (*15*). Often, whether a molecule exhibits an orientational memory is an issue, i.e., whether it preferentially jumps back to its initial orientation (after having performed a jump from one orientation to another one). To address this type of question, three-point correlation functions or three-dimensional spectra have been found useful in previous ^{2}H and ^{13}C NMR experiments (*16, 17*). Information about orientational memories, let alone about effective slow ↔ fast exchange processes, is hardly obtainable directly by any other method.

In the field of solid electrolytes the question of an analogous translational memory, often discussed under the term "correlated back and forth jumps," plays an important role in pertinent theories, see, e.g., Refs. (*18, 19*). Therefore, it would be most useful if multiple time correlation functions could be recorded for nuclei such as ^{7}Li, which play a prominent role in these materials, e.g., in energy storage devices. The present article is devoted to investigating the conditions required to approach this goal. In any case it is encouraging that in many relevant cases ^{7}Li (*20*) and ^{9}Be (*3*), and under favorable conditions also spin-3/2 probes such as ^{11}B (*21*), exhibit rigid lattice spectra that are not broader than those of deuterons. These spectra can thus easily be excited in a nonselective fashion using suitable probe heads and high-power RF transmitters.

It is pointed out that ^{6}Li is a also good probe for the study of the dynamics in ion conductors (*22*). For this isotope the dipolar coupling typically dominates the quadrupolar and chemical shift interactions. This then calls for the application of magic angle spinning and often, due to the low abundance of ^{6}Li, for isotopic enrichment. For ^{7}Li and ^{9}Be probes in solids the quadrupolar coupling is usually by far the strongest. Consequently, for the solid-state stimulated echo experiments mentioned above (*6, 7*) sample rotation techniques were not found to be necessary.

This article is organized as follows: First, we outline a modular design of pulse sequences for the detection of multiple-time correlation functions using nonselectively excitable spin-3/2 nuclei in solids (Section 2.1). Then, in Section 2.2 we present a compact notation for the phase cycles adapted to the present situation. In Section 2.3 we address some problems in obtaining pure longitudinal states. The specific applications then discussed include the well-known Jeener–Broekaert experiment (Section 3.1) and its generalizations to higher multipolar spin orders (Section 3.3). Carried out as stimulated echo spectroscopy, these techniques enable one to correlate NMR frequencies at two points in time. The asymptotic echo behavior in overall isotropic samples, useful when details of motional processes are in question, is also dealt with (Section 3.2). Finally, the conditions for the generation of four-time stimulated echoes (Section 4.1) as well as specific implementations of this multiple-pulse experiment are discussed (Section 4.2). In Section 5 we briefly summarize our findings.

2. GENERAL CONSIDERATIONS

Let us consider the evolution of the density matrix for spin $I = 3/2$ nuclei in nonrotating solids under the action of the first-order quadrupolar Hamiltonian. In the rotating frame it reads, in accord with conventions used by several authors, e.g., Refs. (*1, 23, 24*),

$$H_Q \equiv \frac{1}{\sqrt{6}}\,\omega_Q T_{20}. \qquad [1]$$

Here the spherical tensor operator may also be expressed as $T_{20} = 1/\sqrt{6}\,[3I_z^2 - I(I+1)]$. The quadrupolar frequency is $\omega_Q = \frac{1}{2}\delta(3\cos^2\theta - 1 - \eta\sin^2\theta\cos 2\phi)$ with the polar angle θ and the azimuthal angle ϕ describing the orientation of the EFG tensor at the nuclear site in the usual fashion. $\delta = e^2qQ/2\hbar$ and η denote the anisotropy and asymmetry parameters, respectively. Most of our treatment will be in terms of the standard irreducible spherical tensor operators, T_{lm} (*1, 23*), with $I_x = -1/\sqrt{2}\,(T_{11} - T_{1-1})$ and $I_y = i/\sqrt{2}\,(T_{11} + T_{1-1})$. The normalized tensors are given by $\hat{T}_{lm} = \lambda_l T_{lm}$ with $\lambda_1 = 1/\sqrt{5}$, $\lambda_2 = 1/\sqrt{6}$, and $\lambda_3 = \sqrt{2}/3$ for $I = 3/2$ (*25*).

In the following we will deal with hard and nonselective radiofrequency (RF) pulses, i.e., both the central transition as well as the satellite transitions can be excited. The RF pulses are characterized by a flip angle β and a phase φ and will be designated β_φ. The theoretical framework for the treatment of the effects of finite pulse lengths is well known (*26–29*). But since the gyromagnetic ratios for the nuclei considered here are at least comparable to those of ^{2}H, the delta pulse approximation will usually be well justified.

In the present article no interactions other than those given by Eq. [1] are taken into account. It is pointed out, however, that Tang and Wu have considered, in addition to the quadrupolar interaction, an isotropic shift interaction of the form $H_S = \Delta\omega I_z$ (*30*). H_S is essentially irrelevant for small evolution times t_p, i.e., provided $\Delta\omega/\omega_Q \ll 1$. This condition is fulfilled to a high degree for many typical cases (e.g., with $\Delta\omega$ corresponding to the frequency offset due to an isotropic chemical shift or due to a Knight shift). If longer t_p are a concern then refocusing by a 180° pulse placed in the middle of an evolution period has turned out to be helpful in some situations (*11, 33*), e.g., for cases in which only a small residual (quadrupolar)

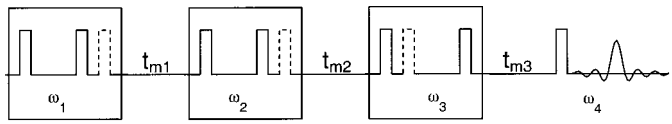

FIG. 1. Modular timing scheme for the generation of multiple time (here: four-time) correlation functions. A unique quadrupolar modulation with frequency ω_i is desired during each module which consists of two to four pulses. Each module is highlighted by a square box. The mixing times, t_{mi}, are also indicated. The final read-out sequence will usually involve one or two pulses.

coupling is present. As a further simplification we will not consider transverse spin-relaxation. It is pointed out, however, that such effects were already studied for spin-3/2 nuclei with vanishing (*8*) and nonvanishing (*11, 31*) quadrupolar couplings.

2.1. Coherence Pathways and Coherence Transfer Amplitudes

The general timing scheme employed in multidimensional solid-state NMR spectroscopy is depicted in Fig. 1. Starting from a longitudinal state, T_{l0}, RF pulses (and in ^{13}C NMR also cross-polarization procedures) are used to generate an alternating sequence of transverse states, $T_{l\pm m}$ (desired during the evolution times, t_p) and longitudinal ones (desired during the mixing times, t_m). It is then convenient to decompose the entire pulse sequence into smaller subunits. The simplest useful units consist of two (or three) pulses with an evolution time (and a purging time) interleaved and a subsequent mixing time. The goal of such a procedure is to obtain a modulated, unique longitudinal state, i.e., one which carries the information on the quadrupolar frequency acquired in the prior evolution time. By combining one or more of those building blocks in conjunction with a read-out sequence, complex multiple-time modulations can be generated in a relatively simple manner.

In order to obtain a well-defined succession of quadrupolar modulations, phase cycling has to be employed. This is to ensure that after each subunit only the desired coherence pathway, associated with a unique quadrupolar encoding, is reconverted back into a longitudinal state or into detectable signal.

Polarization states (T_{l0}) as well as triple-quantum coherences (TQCs, $T_{3\pm3}$) commute with the quadrupolar Hamiltonian, Eq. [1]. Therefore, for the generation of modulated states during the evolution times in the present context one aims at selecting a path with either $m = 1$ (single quantum, SQ, modulation) or, if possible, $m = 2$ (double quantum, DQ, modulation). Corresponding partial coherence transfer pathways are shown in Figs. 2, 3, and 4. Most simple are those SQ pathways leading to a final quadrupolar state (Fig. 2b). The ones yielding pure octupolar order, T_{30}, require three pulses (Fig. 3a). They involve an intermediate TQC as a purging state if one intends a flip-angle-independent elimination of T_{10} (which otherwise would occur together with T_{30}). Two population states with $l > 1$ can be connected via DQ encoding

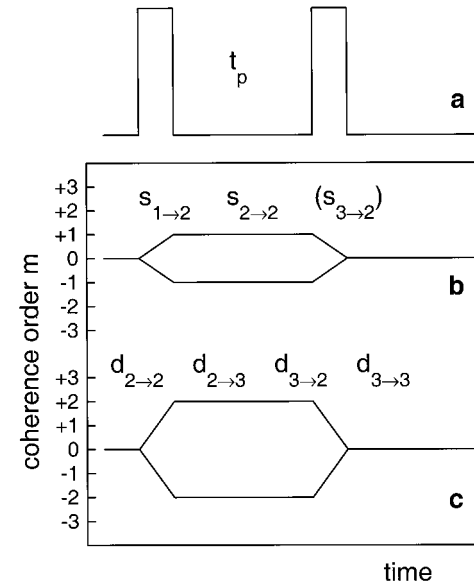

FIG. 2. Schematic representation of (a) pulse sequence and of partial coherence transfer pathways showing how initial (T_{l0}) and final ($T_{l'0}$) population states may be connected for simple (b) SQ and (c) DQ encoding. One of the coherence transfer amplitudes ($s_{3\to2}$) which may be of minor importance is put in parentheses.

according to the diagram shown in Fig. 2c or, alternatively, Fig. 3c. In some cases, to be discussed in Section 2.3, below, it may be advisable to implement also a TQ filter prior to the quadrupolar encoding; some examples are depicted in Fig. 4. In the following, except for the detection period, we will consider symmetrical coherence pathway diagrams only, since single

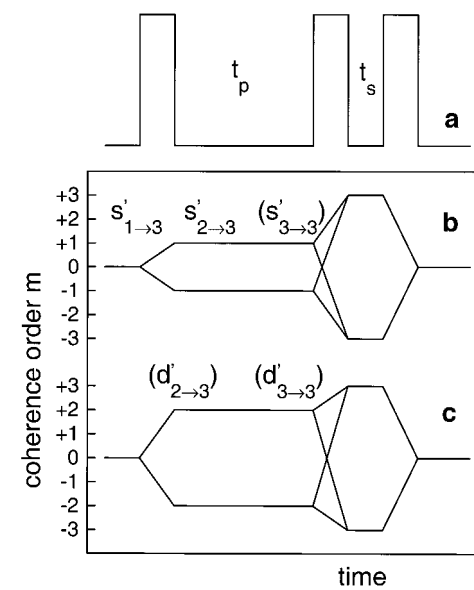

FIG. 3. (a) Pulse sequence and (b, c) partial coherence transfer pathway diagrams for the generation of modulated T_{30} states with one (final) TQ filtration period interleaved.

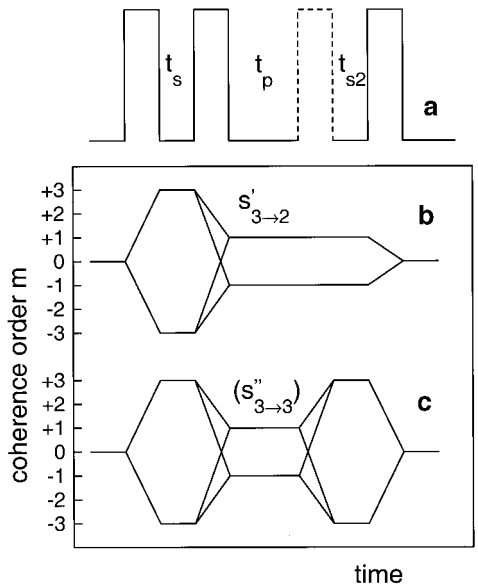

FIG. 4. (a) Pulse sequence and partial coherence transfer pathway diagrams associated with the amplitudes (b) $s'_{3\to 2}$ (requiring three pulses) and (c) $s''_{3\to 3}$ (requiring four pulses and an additional purging period t_{s2}). The TQ filtration prior to the evolution period may be useful for eliminating the relaxation induced contamination of the initial octupolar order. The analogous DQ diagrams are not shown.

paths are usually associated with smaller coherence transfer amplitudes.

The coherence transfer amplitudes arising from the interactions considered here are well known: (i) The transfer induced by the RF pulses can conveniently be described by the Wigner rotation matrix. General expressions and tabulated values of the corresponding matrix elements are given in many places, e.g., Refs. (*1*, *24*, *32*). (ii) The evolution under the first-order quadrupolar interaction can be written using the arrow notation (*25*, *33*) as

$$\hat{T}_{lm} \xrightarrow{H_Q t} g^{(m)}_{l'l}(\omega_Q t)\hat{T}_{l'm}. \qquad [2]$$

The quadrupolar precession functions $g^{(m)}_{l'l}(\omega_Q t)$ (with $|m| \le l$ and l') corresponding to this unitary transformation have also been presented by numerous authors in various forms (*8*, *9*, *11*, *23*, *25*, *26*, *30*, *31*, *33*, *34*). For convenience, in Table 1 we reproduce the SQ and DQ modulation factors (in the absence of relaxation effects) as the symmetric matrices $\mathbf{g}^{(+1)}$ and $\mathbf{g}^{(+2)}$. Further matrices may be generated via the relation $g^{(+m)}_{l'l}(\omega_Q t) = (-1)^{l-l'} g^{(-m)}_{l'l}(\omega_Q t)]$.

The coherence transfer pathways depicted in Figs. 2, 3, and 4 involve a succession of transfer steps. From these the coherence transfer amplitudes for paths connecting two longitudinal states may be computed. For SQ and DQ encoding we will denote the composite coherence transfer amplitudes as $s_{l\to l'}$ and $d_{l\to l'}$, respectively. More precisely they may be defined in shorthand notation for SQ encoding from $T_{l0} \to s_{l\to l'} T_{l'0}$ and for DQ encoding from $T_{l0} \to d_{l\to l'} T_{l'0}$. When using normalized tensor operators one may analogously write $\hat{T}_{l0} \to \hat{s}_{l\to l'}\hat{T}_{l'0}$ or $\hat{T}_{l0} \to \hat{d}_{l\to l'}\hat{T}_{l'0}$ and hence $\hat{s}_{l\to l'} = s_{l\to l'}\lambda_l/\lambda_{l'}$ and $\hat{d}_{l\to l'} = d_{l\to l'}\lambda_l/\lambda_{l'}$. In Figs. 2 through 4 we show several transfer amplitudes along with the corresponding pathway diagrams. Dashed quantities (e.g., $s'_{l\to l'}$ and $d'_{l\to l'}$) signal that intermediate TQCs are involved. The transfer amplitudes shown in brackets in Figs. 2, 3, and 4 are of minor importance, for reasons to be discussed below, but are nevertheless included for illustration purposes.

From the Wigner rotation matrix elements and the quadrupolar modulation factors it is a simple matter to compute various useful coherence transfer amplitudes ($s_{l\to l'}$, $d_{l\to l'}$, etc.). Corresponding results are given in Table 2 where we also specify the flip angles which maximize the transfer amplitudes. The corresponding maximum transfer amplitudes, denoted there as $T_{\max}$, are reported in Table 2 as well.

To provide an example for these computations let us consider the DQ modulation coefficient for connecting two quadrupolar spin-alignment states ($l = l' = 2$). Adding the results from the coherence paths with $m = 2$ and $m = -2$ one obtains $\hat{d}_{2\to 2} = [d^2_{02}(\beta_2) g^2_{22}(\omega_Q t) d^2_{20}(\beta_1) + d^2_{0-2}(\beta_2) g^{-2}_{22}(\omega_Q t) d^2_{-20}(\beta_1)]$. From the properties of the reduced Wigner rotation matrix elements, $d^{(l)}_{m'm}(\beta)$, and the coefficients given in Table 1 this yields $d_{2\to 2} = 2d^2_{02}(\beta_2) g^2_{22}(\omega_Q t) d^2_{20}(\beta_1) = \frac{3}{4}\sin^2\beta_1 \sin^2\beta_2 \cos(\omega_Q t)$. The flip angles β which maximize this transfer amplitude are evident from this expression.

During t_p the transverse states for $I \le 1$ nuclei are modulated solely by $\sin(\omega_Q t_p)$ or by $\cos(\omega_Q t_p)$ factors, see, e.g., Ref. (*1*). As Table 1 (and 2) shows, for spin-3/2 nuclei three additional coefficients show up. These are $g^{(1)}_{11}(\omega_Q t) \propto 3\cos(\omega_Q t) + 2 = \frac{1}{2}[3\exp(i\omega_Q t) + 4\exp(0) + 3\exp(-i\omega_Q t)]$, $g^{(1)}_{13}(\omega_Q t) \propto \cos(\omega_Q t) - 1 = \frac{1}{2}[\exp(i\omega_Q t) - 2\exp(0) + \exp(-i\omega_Q t)]$, and $g^{(1)}_{33}(\omega_Q t) \propto 2\cos(\omega_Q t) + 3$. The former

TABLE 1
Quadrupolar Modulation Factors, $g^{(m)}_{l'l}(\omega_Q t)$, as Defined in Eq. [2] for $m = +1$ (Top) and $m = +2$ (Bottom)

$g^{(1)}_{l'l}(\omega_Q t)$	$l = 1$	$l = 2$	$l = 3$
$l' = 1$	$\frac{1}{5}[3\cos(\omega_Q t) + 2]$	$-i\sqrt{\frac{3}{5}}\sin(\omega_Q t)$	$\sqrt{6}/5\,[\cos(\omega_Q t) - 1]$
$l' = 2$	$-i\sqrt{\frac{3}{5}}\sin(\omega_Q t)$	$\cos(\omega_Q t)$	$-i\sqrt{\frac{2}{5}}\sin(\omega_Q t)$
$l' = 3$	$\sqrt{6}/5\,[\cos(\omega_Q t) - 1]$	$-i\sqrt{\frac{2}{5}}\sin(\omega_Q t)$	$\frac{1}{5}[2\cos(\omega_Q t) + 3]$

$g^{(2)}_{l'l}(\omega_Q t)$	$l = 2$	$l = 3$
$l' = 2$	$\cos(\omega_Q t)$	$-i\sin(\omega_Q t)$
$l' = 3$	$-i\sin(\omega_Q t)$	$\cos(\omega_Q t)$

Note. These quadrupolar modulation factors show up along the paths connecting an initial state of rank l via m quantum encoding to a final rank l' coherence.

TABLE 2

Path	Coherence transfer amplitude	β_1	β_2	β_3	T_{max}	Pulse sequence	$\sigma = (-1)^K$; $K =$
$s_{1\to2}$	$-\frac{1}{2}\sqrt{\frac{3}{2}}\sin\beta_1\sin 2\beta_2\sin(\omega_Q t_p)$	90°	45°	—	$-\frac{1}{2}\sqrt{\frac{3}{2}}\sin(\omega_Q t_p)$	$(X_{k_{2,1}\pi}$–t_p–$Y_{k_{2,2}\pi})_{k_{4,3}\pi/2}$	$k_{2,1} + k_{2,2}$
$s'_{1\to3}$	$-\frac{1}{2}\sqrt{\frac{5}{2}}\sin\beta_1\sin^2\beta_2\sin^3\beta_3\sin^2(\omega_Q t_p/2)$	90°	90°	90°	$-\frac{1}{2}\sqrt{\frac{5}{2}}\sin^2(\omega_Q t_p/2)$	$((X_{k_{2,1}\pi}$–t_p–$Y_{k_{2,2}\pi})_{k_{6,4}\pi/3}$–$t_s$–$X_{k_{2,3}\pi})_{k_{4,5}\pi/2}$	$k_{2,1} + k_{2,3} + k_{6,4}$
$s_{2\to1}$	$-\frac{3}{5}\sqrt{\frac{3}{2}}\sin 2\beta_1\sin\beta_2\sin(\omega_Q t_p)$	45°	ψ_{63}	—	$-\frac{3}{5}\sqrt{\frac{6}{5}}\sin(\omega_Q t_p)$	$(X_{k_{2,1}\pi}$–t_p–$Y_{k_{2,2}\pi})_{k_{4,3}\pi/2}$	—
$s_{2\to2}$	$-\frac{3}{4}\sin 2\beta_1\sin 2\beta_2\cos(\omega_Q t_p)$	45°	45°	—	$-\frac{3}{4}\cos(\omega_Q t_p)$	$(X_{k_{2,1}\pi}$–t_p–$X_{k_{2,2}\pi})_{k_{4,3}\pi/2}$	$k_{2,1} + k_{2,2}$
$s'_{2\to3}$	$+\sqrt{15}/8\sin 2\beta_1\sin^2\beta_2\sin^3\beta_3\sin(\omega_Q t_p)$	45°	90°	90°	$+\sqrt{15}/8\sin(\omega_Q t_p)$	$((X_{k_{2,1}\pi}$–t_p–$X_{k_{2,2}\pi})_{k_{6,4}\pi/3}$–$t_s$–$Y_{k_{2,3}\pi})_{k_{4,5}\pi/2}$	$k_{2,1} + k_{2,3} + k_{6,4}$
$s_{2\to det}$	$\frac{3}{5}\sqrt{\frac{3}{2}}\sin 2\beta_1\sin(\omega_Q t)$	45°	—	—	$\frac{3}{5}\sqrt{\frac{3}{2}}\sin(\omega_Q t)$	$X_{k_{2,1}\pi}$–t–acquisition	$k_{2,1}$
$s'_{3\to2}$	$+9\sqrt{5}/64\sin^3\beta_1\sin^2\beta_2\sin 2\beta_3\sin(\omega_Q t_p)$	90°	90°	45°	$+9\sqrt{5}/64\sin(\omega_Q t_p)$	$((X_{k_{6,1}\pi/3}$–t_p–$Y_{k_{2,2}\pi})_{k_4\pi/6}$–$t_s$–$X_{k_{2,3}\pi})_{k_{4,5}\pi/2}$	$k_{6,1} + k_{2,3}$
$s_{3\to det}$	$9/5\sqrt{10}\sin\beta_1(4 - 5\sin^2\beta_1)\sin^2(\omega_Q t/2)$	ψ_{31}	—	—	$8\sqrt{6}/25\sin^2(\omega_Q t/2)$	$X_{k_{2,1}\pi}$–t–acquisition	$k_{2,1}$
$s'_{3\to det}$	$9/4\sqrt{10}\sin^3\beta_1\sin^2\beta_2\sin^2(\omega_Q t/2)$	90°	90°	—	$9/4\sqrt{10}\sin^2(\omega_Q t/2)$	$X_{k_{6,1}\pi/3}$–t_p–$Y_{k_{2,2}\pi}$–t–acquisition	$k_{6,1}$
$d_{2\to2}$	$+\frac{3}{4}\sin^2\beta_1\sin^2\beta_2\cos(\omega_Q t_p)$	90°	90°	—	$+\frac{3}{4}\cos(\omega_Q t_p)$	$(X_{k_{4,1}\pi/2}$–t_p–$Y_{k_{2,2}\pi})_{k_{4,3}\pi/2}$	$k_{6,1}$
$d_{2\to3}$	$-\sqrt{15}/2\sin^2\beta_1\cos\beta_2\sin^2\beta_2\sin(\omega_Q t_p)$	90°	ψ_{55}	—	$-\sqrt{5}/3\sin(\omega_Q t_p)$	$(X_{k_1\pi/4}$–t_p–$X_{k_{2,2}\pi})_{k_{4,3}\pi/2}$	$(k_1 - 1)/2$
$d_{3\to2}$	$-3\sqrt{15}/8\cos\beta_1\sin^2\beta_1\sin^2\beta_2\sin(\omega_Q t_p)$	ψ_{55}	90°	—	$-\sqrt{5}/4\sin(\omega_Q t_p)$	$(X_{k_1\pi/4}$–t_p–$Y_{k_{2,2}\pi})_{k_{4,3}\pi/2}$	$(k_1 - 1)/2$
$d_{3\to3}$	$+\frac{15}{4}\cos\beta_1\sin^2\beta_1\cos\beta_2\sin^2\beta_2\cos(\omega_Q t_p)$	ψ_{55}	ψ_{55}	—	$+\frac{5}{9}\cos(\omega_Q t_p)$	$(X_{k_{4,1}\pi/2}$–t_p–$Y_{k_{2,2}\pi})_{k_{4,3}\pi/2}$	$k_{4,1}$

Note. Various coherence transfer amplitudes and examples of associated pulse sequences for connecting from a polarization state of rank l to one with rank l' or to detectable signal. Written in terms of the (nonnormalized) spherical tensor operators, $T_{l0} \to s_{l\to l'}T_{l'0}$ and $T_{l0} \to d_{l\to l'}T_{l'0}$ correspond to SQ and DQ encoding, respectively. Also given are the flip angles for maximum transfer, T_{max}, and the partial receiver phases, σ, defined in terms of the phase incrementation parameters $k_{N,i}$, cf. Eq. [3]. Note that $\psi_{31} \equiv \arccos\sqrt{\frac{11}{15}} \approx 31.1°$, $\psi_{55} \equiv \arccos\sqrt{\frac{1}{3}} \approx 54.7°$, and $\psi_{63} \equiv \arccos\sqrt{\frac{1}{5}} \approx 63.4°$. Phase factors for paths terminating at the detection level are not specified. For s_{12} a phase setting is not shown because its implementation requires an ideal flip angle β_2.

two constitute the observable signals induced via a single RF pulse from a pure rank 1 polarization [$M_1(t) \propto g_{11}^{(1)}(\omega_Q t)$] or a rank 3 polarization [$M_3(t) \propto g_{13}^{(1)}(\omega_Q t) \propto s_{3\to det}$, cf. Table 2], respectively. During the mixing time prior to detection pure quadrupolar order (T_{20}) should be present if a simple $\sin(\omega_Q t)$ modulation is desired, cf. Table 1. Likewise at the beginning of the experiment (i.e., starting from T_{10}) this simple quadrupolar encoding is only obtained if $l' = 2$. A glance at Table 1 reveals that $\sin(\omega_Q t_p)$ dependences generally are only obtained for $\Delta l \equiv |l - l'| = 1$, which is important to keep in mind when it comes to the design of four-time correlations as outlined in Section 4, below.

Throughout this article we will for simplicity assume ω_Q to be constant during each evolution period, t_p. Should this not be the case then $\omega_Q t_p$ in the corresponding expressions [e.g., $\sin(\omega_Q t_p)$], is to be replaced by the phase $\Omega \equiv \int_0^{t_p} \omega_Q(s)ds$ for each evolution period.

2.2. Notation for Phase Cycles

In order to be able to generate a unique modulated longitudinal state, i.e., to eliminate contributions from unwanted coherence pathways, phase cycling is essential. In their seminal work Bodenhausen *et al.* (*35*) have formulated the general rules which enable the construction of a phase cycle from a given coherence pathway diagram; see also Refs. (*33, 36*). It is nevertheless often desirable to provide explicit pulse and receiver phase lists for implementation in a laboratory experiment. This requirement typically results in lengthy phase listings, see, e.g., Refs. (*11, 16*). Therefore, in the present subsection we will introduce a notation for phase cycles which allows one to write complex phase lists in a compact manner. At the same time our approach exploits the fact that we use *symmetric* coherence pathway diagrams while complying with the phase cycling rules of Ref. (*35*) in a straightforward manner.

In the present article we consider only amplitude modulated signals (corresponding to symmetrical coherence pathways). Therefore, the receiver phase, except for its sign, can be considered well defined. In keeping with the usual convention we will assume that the coherence pathway terminates at the coherence level -1, although the notion of rotating and counterrotating frames refers to phase-modulated signals and hence is not required in our case as long as, e.g., shift interactions are not relevant. When dealing with partial coherence transfer pathways (such as shown in Figs. 2 through 4) it is convenient to define partial receiver phases, σ, as previously used in the context of stimulated deuteron echo spectroscopy (*37*). Eventually, the overall receiver phase setting, σ_{det}, can be calculated as the product of all partial receiver phases.

In writing down phase cycles it is important to keep track of the phase incrementation of a unit i (i.e., of a pulse, P, or a group of pulses, G) which usually will be in steps of $\varphi_i = k_{N,i}2\pi/N_i$ with (*33, 35*)

$$k_{N,i} = 0, 1, \ldots, N - 1. \qquad [3]$$

In our notation we symbolize the phase incrementation of building block i simply as P_{φ_i} or G_{φ_i}. Thus $P_{k_{2,i}2\pi/2} = P_{k_{2,i}\pi}$ (e.g., with $P \in \{X, Y\}$) implies alternating the phase of pulse i in a twofold cycle ($N_i = 2$ and $k_{2,i} = 0, 1$) from φ to $\varphi + 2\pi/2$. Exploiting the symmetry of the reduced Wigner matrix elements, $d_{m'm}^{(l)}(\beta) = (-1)^{m'-m}d_{m'm}^{(l)}(-\beta)$ (*32*), this is equivalent to referring to rotations with flip angles $+\beta$ and $-\beta$

without changing the pulse phase, φ. In our notation we do not explicitly refer to the flip angles. They only determine the amplitude of the coherence transfer and not the general type of signal filtered out by a phase cycle.

In order to see the present notation in the context of the general phase cycling rules of Ref. (*35*), let us note that $P_{k_{2,i}\pi}$ together with the partial receiver phase $\sigma = (-1)^{k_{2,i}}$ signals an odd change in coherence order $T_{lp} \rightarrow T_{lp'}$ with $\Delta p \equiv p' - p = \pm 1, \pm 3, \pm 5, \pm 7, \ldots$, as typically required in SQ encoding. $P_{k_{2,i}\pi}$ in conjunction with $\sigma = 1 = (-1)^0$ marks an even Δp $(= 0, \pm 2, \pm 4, \pm 6, \cdots)$ as one of the ingredients required for DQ encoding. As we will see below in some cases another twofold cycling may turn out to be helpful: Using $P_{k_i\pi/(2q)}$ with $k_i = -1, 1$ and $\sigma = k_i = (-1)^{(k_i-1)/2}$ one can select a multiple quantum coherence (MQC) of order q. Furthermore, $N_i = 4$ the expression $(G)_{k_{4,i}2\pi/4}$ with $\sigma = 1$ employing the rules formulated in Ref. (*35*) yields $\Delta p = 0, \pm 4, \pm 6, \ldots$. Analogously $N_i = 6$ or $(G)_{k_{6,i}2\pi/6}$ with $\sigma = (-1)^{k_{6,i}}$ selects $\Delta p = \pm 3, \ldots$. This way of writing the partial receiver phases is particularly useful for the computerized generation of phase lists.

A more complex example for our notation is the phase cycle $(X_{k_{2,1}\pi} - t_p - Y_{k_{2,2}\pi})_{k_{4,3}\pi/2}$ together with the partial receiver phase $\sigma = (-1)^{k_{2,1}}(-1)^{k_{2,2}}$. When starting from Zeeman order this cycle corresponds to the sine-modulated transfer amplitude $s_{1\rightarrow 2}$ (cf. Table 2) and the pathway diagram shown in Fig. 2b. Here, the symbols X and Y in the group of pulses $G = X_{k_{2,1}\pi} - t_p - Y_{k_{2,2}\pi}$ mark that the phase difference between the first and the second pulse is $|\varphi_1 - \varphi_2| = 90°$. Examples for phase cycles and associated partial receiver phase settings corresponding to various other transfer pathways are given in Table 2.

It should be noted that, as usual, the phase alternation or incrementation of all units proceeds independent of one another. The phase list for a given experiment is then obtained by nesting all partial phase lists. Thus the number of scans within a cycle is given by the product of all N_i. However, in many cases a reduction of the phase cycle to a smaller length will be possible (*35, 38*). In solids the lifetime of transverse states is usually much shorter than that of the populations. This is often exploited also, e.g., in deuteron stimulated echo spectroscopy to reduce the length of a phase cycle even further by choosing the mixing times, t_m, sufficiently long.

2.3. Generation of Pure, Modulated Longitudinal States

During the detection period we will only have to consider the evolution and hence quadrupolar modulation of just one SQC if, during the last mixing time of an experiment, a unique longitudinal state existed. In particular it is difficult to create a pure, modulated Zeeman order unless the flip angles are set exactly to their nominal values (which is hard to achieve in practice). To illustrate this statement in connection with SQ encoding let us recall that from any single SQC, T_{l1}, present right after an initial pulse all three $T_{l'1}$ states (those with $l' = 1$, 2, and 3) will evolve. Phase cycling of the second pulse will only facilitate the separation of a quadrupolar ordered state from those with odd l', i.e., T_{10} cannot be separated from T_{30} by symmetry alone.

However, assuming ideal flip angles it is possible to separate Zeeman order, T_{10}, from octupolar order, T_{30}. For an estimate of how well defined the flip angles have to be set in order to accomplish such a separation let us consider the total transfer amplitudes, $s_{l\rightarrow l'}$, for the two SQ pathways which are in shorthand notation described by $T_{20} \rightarrow s_{2\rightarrow 1}T_{10}$ and $T_{20} \rightarrow s_{2\rightarrow 3}T_{30}$. The associated amplitude factors are $s_{2\rightarrow 1} = -\frac{3}{5}\sqrt{\frac{3}{2}}\sin 2\beta_1 \sin\beta_2 \sin(\omega_Q t_p)$ (cf. Table 2) and $s_{2\rightarrow 3} = \frac{1}{2}\sqrt{\frac{3}{5}}\sin 2\beta_1 \sin\beta_2(4 - 5\sin^2\beta_2)\sin(\omega_Q t_p)$. From the latter expression one recognizes that $s_{2\rightarrow 3} = 0$ for a flip angle $\beta_2 = \arccos\sqrt{\frac{1}{5}} \approx 63.4°$. For this β_2 (together with $\beta_1 = 90°$) the coefficient $s_{2\rightarrow 1}$ is still about 80% of its maximum. The ratio $s_{2\rightarrow 3}/s_{2\rightarrow 1}$ thus obtained is $\frac{1}{3}\sqrt{\frac{5}{2}}(4 - 5\sin^2\beta_2)$. Consequently, for a pulse length mismatch of 3°, corresponding to an inhomogeneity of the RF pulse amplitude of ≈5%, the amplitude of T_{30} is already about 10% compared to that of T_{10}. Thus pure, quadrupolar modulated Zeeman states can only be generated under favorable conditions. Therefore, additional ways of suppressing octupolar order may become necessary and will be discussed further below.

The generation of pure octupolar order is easily possible via an intermediate TQC, at least for initial polarization states with $l < 3$: The only polarization state which can be generated from $T_{3\pm 3}$ via a hard RF pulse is the octupolar ordered one, cf. Fig. 3. However, if T_{30} is required to be the initial state (cf. Fig. 4) then it is likely to be contaminated by Zeeman order. The latter then has to be removed in order to ensure a unique quadrupolar modulation. Such a contamination limits the utility of the pathways associated with the coefficients which therefore appear in brackets in Figs. 2b and 3b. Unwanted T_{10} admixtures can arise from quadrupolar spin–lattice relaxation taking place during sufficiently long mixing times, t_m. In the nomenclature of Refs. (*8, 25*) this may be written as $\hat{T}_{30} \xrightarrow{R^{(0)}} f_{13}^{(0)}(t_m)\hat{T}_{10} + f_{33}^{(0)}(t_m)\hat{T}_{30}$. The longitudinal relaxation functions are given by $f_{13}^{(0)}(t_m) = \frac{2}{5}[-\exp(-R_3^{(0)}t_m) + \exp(-R_4^{(0)}t_m)] = f_{31}^{(0)}(t_m)$ and $f_{33}^{(0)}(t_m) = \frac{1}{5}[\exp(-R_3^{(0)}t_m) + 4\exp(-R_4^{(0)}t_m)]$. The rates $R_3^{(0)} = 2CJ_2$ and $R_4^{(0)} = 2CJ_1$ are defined in terms of the spectral densities J_n and the quadrupolar coupling constant C, cf. Ref. (*8*). Elimination of the unwanted T_{10} admixture can be achieved by an initial TQ filter as depicted in Fig. 4. Consequently for the transfer $T_{30} \rightarrow s''_{3\rightarrow 3}T_{30}$ two TQ filters are advisable (Fig. 4c). Since the relaxation of quadrupolar order is single exponential, $\hat{T}_{20} \xrightarrow{R^{(0)}} f_{22}^{(0)}(t_m)\hat{T}_{20}$, corresponding measures should not be required in this case. Furthermore, DQ encoding starting from initial T_{30} will not require filtration analogous to the situation shown in Fig. 4 since a single hard pulse cannot yield DQCs from Zeeman order anyway (therefore we have put the corresponding coefficients in Fig. 3c in brackets).

3. TWO-TIME CORRELATION FUNCTIONS

3.1. The Jeener–Broekaert Experiment

This type of experiment was first devised for the creation of dipolar order in spin-$\frac{1}{2}$ systems (*39*). Nowadays it is in widespread use for deuteron NMR studies of solids (*1*), for MQ filter experiments on quadrupolar spin systems in liquid-like environments (*11, 40*), and most recently for the detection of ultraslow motion in inorganic materials using spin-3/2 nuclei (*6, 7*). Therefore, it might suffice to discuss this experiment very briefly.

Starting from equilibrium longitudinal magnetization, $I_z = T_{10}$, the quadrupolar alignment state can be generated from $T_{10} \xrightarrow{\beta_1 I_{\varphi 1}} \xrightarrow{H_Q t_p} \xrightarrow{\beta_2 I_{\varphi 2}} s_{1\to 2} T_{20}$ if $|\varphi_1 - \varphi_2| = 90°$. Then, after the mixing time the transfer into observable magnetization, M_φ, is accomplished via $T_{20} \xrightarrow{\beta_3 I_{\varphi 3}} \xrightarrow{H_Q t} s_{2\to \mathrm{det}} M_{\varphi 3}$. The arbitrary phase φ_3 specifies the direction along which the useful signal shows up upon detection. If, as assumed in Table 2, we employ an X pulse for $s_{2\to\mathrm{det}}$ then the amplitude modulated signal appears as x magnetization M_x (i.e., $M_x \propto I_x$).

The product of the associated modulation factors, $-s_{1\to 2} s_{2\to \mathrm{det}}$, see Table 2, yields the overall coherence transfer amplitude, i.e., the magnitude of the sin–sin signal as

$$S_2(t_\mathrm{p}, t_\mathrm{m}, t) = \tfrac{9}{20} \sin\beta_1 \sin 2\beta_2 \sin 2\beta_3 \sin[\omega_\mathrm{Q}(0) t_\mathrm{p}] \sin[\omega_\mathrm{Q}(t_\mathrm{m}) t]. \quad [4]$$

Thus S_2 will be maximum if the flip angles are chosen as $\beta_1 = 90°$ and $\beta_2 = \beta_3 = 45°$. For $t = t_\mathrm{p}$ a pure quadrupolar spin-alignment echo should be observed in powders even if the flip angles (i.e., the amplitudes of the RF pulses) are not well defined across the sample. In the notation defined above the entire pulse sequence may be written as $(X_{k_{2,1}\pi}\text{–}t_\mathrm{p}\text{–}Y_{k_{2,2}\pi})_{k_{4,4}\pi/2}\text{–}t_\mathrm{m}\text{–}X_{k_{2,3}\pi}\text{–}t$–acquisition with $\sigma_\mathrm{det} = (-1)^{k_{2,1}+k_{2,2}+k_{2,3}}$; cf. Table 2. Note that here we have first numbered the three pulses in turn and then the pulse incrementation parameter, $k_{4,i=4}$, associated with the DQ elimination.

In order to illustrate further the notation for the setting of the receiver phase, let us suppose that we wish to study how DQCs decay during t_m. Then, one could use the latter pulse sequence together with $\sigma_\mathrm{det} = (-1)^{k_{2,1}+k_{2,2}+k_{2,3}+k_{4,4}}$.

3.2. Asymptotic Correlations in Powders

Analogous to the situation for spins $I \le 1$ the sin–sin signal, Eq. [4], may be helpful in recording two-dimensional NMR spectra (*1*). Furthermore, quadrupolar spin-alignment echoes have been extensively employed in order to determine the time scale of dynamic processes and to elucidate the geometry of motional mechanisms in powder samples. In the latter respect

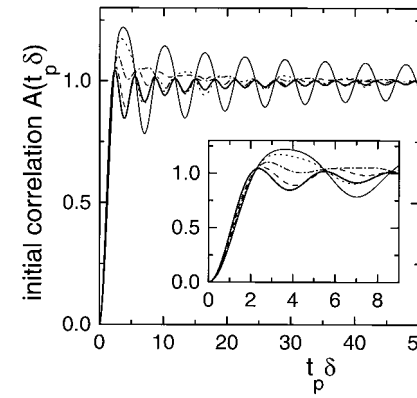

FIG. 5. Initial correlation, $A^{\mathrm{SIN}}(t_\mathrm{p}\delta)$, calculated using Eq. [5] for various asymmetry parameters: $\eta = 0$ (thin solid line), 0.25 (dotted line), 0.5 (dash–dotted line), 0.75 (dashed line), and 1 (thick solid line). The inset provides a magnified view for small $t_\mathrm{p}\delta$.

the initial and final state amplitudes, i.e., $A^{\mathrm{SIN}}(t_\mathrm{p}) \equiv \langle S_2(t_\mathrm{p}, t_\mathrm{m} \to 0, t_\mathrm{p})\rangle / \langle S_2(t_\mathrm{p} \to \infty, t_\mathrm{m} \to 0, t_\mathrm{p} \to \infty)\rangle$ and $Z^{\mathrm{SIN}}(t_\mathrm{p}) \equiv \langle S_2(t_\mathrm{p}, t_\mathrm{m} \to \infty, t_\mathrm{p})\rangle / \langle S_2(t_\mathrm{p}, t_\mathrm{m} \to 0, t_\mathrm{p})\rangle$, respectively, are of interest (*41, 42*). The specification $t_\mathrm{p} \to \infty$ means that the sequence of conditions $\delta^{-1} \ll t_\mathrm{p} \ll \tau_\mathrm{C} \ll t_\mathrm{m}$ (with τ_C denoting a characteristic correlation time) should be fulfilled.

The initial correlation can be calculated via

$$A^{\mathrm{SIN}}(t_\mathrm{p}) = \frac{1}{2\pi} \langle \sin^2[\omega_\mathrm{Q}(\theta, \phi) t_\mathrm{p}]\rangle \equiv \frac{1}{2\pi} \int_0^{2\pi} d\phi \int_0^{\pi} d\theta \, \sin\theta \sin^2[\omega_\mathrm{Q}(\theta, \phi) t_\mathrm{p}] \quad [5a]$$

$$= 1 - \int_0^{\pi/2} d\theta \, \sin\theta J_0(t_\mathrm{p}\delta\eta \sin^2\theta) \times \cos[t_\mathrm{p}\delta(3\cos^2\theta - 1)]. \quad [5b]$$

In Eq. [5b] the Bessel function, $J_0(x) \equiv x^{-1}\sin x$, stems from integrating over the azimuthal angle, ϕ. For $t_\mathrm{p}\delta \to 0$ and hence $J_0 \to 1$ one finds that $A^{\mathrm{SIN}}(t_\mathrm{p})$ should be independent of the asymmetry parameter, η. Furthermore, for small $t_\mathrm{p}\delta$ the outer cosine function in Eq. [5b] can be expanded to yield $A^{\mathrm{SIN}}(t_\mathrm{p}) \propto (t_\mathrm{p}\delta)^2$. In Fig. 5 we show $A^{\mathrm{SIN}}(t_\mathrm{p})$ for several asymmetry parameters. $A^{\mathrm{SIN}}(t_\mathrm{p})$ is seen to be practically independent of η up to about $t_\mathrm{p}\delta = 2$. Note that the analogously defined quantity $A^{\mathrm{COS}}(t_\mathrm{p}) \equiv \frac{1}{2\pi}\langle \cos^2[\omega_\mathrm{Q}(\theta, \phi) t_\mathrm{p}]\rangle$ is related to $A^{\mathrm{SIN}}(t_\mathrm{p})$ via $A^{\mathrm{COS}}(t_\mathrm{p}) = 2 - A^{\mathrm{SIN}}(t_\mathrm{p})$.

Since Eq. [5] is independent of the nuclear spin, I, it is useful for other cases with $\eta \neq 0$ as well (e.g., ^{13}C NMR). However, an important difference to most applications with $I \le 1$ has to be mentioned. For $I \le 1$ probes (often being part of a covalent bond) motional processes usually lead to a reorien-

tation of the interaction tensor while leaving the numerical values of δ and η invariant. For the $I = 3/2$ probes we have in mind (here ionic bonding is more familiar) such a behavior can be expected to be the exception rather than the rule. This is because ionic (translational) motions will in general occur between unlike sites, i.e., those for which the field gradient tensors are not simply related via rotations. In this latter case the initial correlation is given by the weighted sum of $A^{\mathrm{SIN}}(t_{\mathrm{p}})$ contributions evaluated for the various tensor parameters. Such a superposition will in general dampen out the oscillatory behavior seen in Fig. 5.

Similarly, the final state correlation factors, $Z^{\mathrm{SIN}}(t_{\mathrm{p}})$, in general will involve contributions from several unlike sites. Then a comparatively structureless evolution time dependence of Z^{SIN} may be expected for t_{p} not much longer than the inverse average quadrupolar coupling: The existence of several coupling constants should lead to a beating in Z^{SIN}. Furthermore, analogous to the "smoothing" seen for A^{SIN} when increasing η (cf. Fig. 5) for Z^{SIN} a similar effect may be expected. More important is probably the asymptotic behavior of the final state amplitude which has been found very useful, e.g., in deuteron NMR studies (*41*). It turns out that $1/Z^{\mathrm{SIN}}(t_{\mathrm{p}} \rightarrow \infty)$ reflects the number, n, of accessible, magnetically inequivalent sites, provided they are equally populated (*41*). If the latter restriction is lifted, then this result can be generalized to

$$Z^{\mathrm{SIN}}(t_{\mathrm{p}} \rightarrow \infty) = \sum_{i=1}^{n} w_i^2. \qquad [6]$$

Here the summation runs over the different sets, i, of tensor parameters (δ_i, η_i) and w_i are the corresponding weighting factors for each magnetically inequivalent site. In order to justify the latter expression one should realize that for sufficiently large t_{p} only those contributions will appear in the echo for which the phases, Ω, acquired prior as well as subsequent to the mixing time, exhibit exactly the same absolute value. We then arrive at the above expression by noting that the joint probability for finding a particle in a given orientation at site i prior *and* subsequent to t_{m} is equal to the square of the equilibrium occupancy of this site. Applying this argument for each magnetically inequivalent site yields the above results if we take into account that in a powder (an overall isotropic sample) the contributions from those coherences exhibit negligible weight which *accidentally* acquire the same phase during the two evolution times. As an example for such a coincidence, consider an axially symmetric interaction tensor with the largest principal axis, e.g., a C–D bond, moving on the mantle of a cone with the cone axis accidentally oriented along the magnetic field.

In the above considerations we have implicitly assumed the existence of a *finite* number, n, of inequivalent sites per unit cell, i.e., the case of a polycrystal. In an amorphous material with a practically infinite number of sites one has $Z^{\mathrm{SIN}}(t_{\mathrm{p}} \rightarrow \infty) \rightarrow 0$. Since the above expression for $Z^{\mathrm{SIN}}(t_{\mathrm{p}} \rightarrow \infty)$ rests only on probability considerations, Eq. [6] holds as well for the analogously defined quantity $Z^{\mathrm{COS}}(t_{\mathrm{p}} \rightarrow \infty) \equiv \langle \cos[\omega_{\mathrm{Q}}(0)t_{\mathrm{p}}]\cos[\omega_{\mathrm{Q}}(t_{\mathrm{m}} \rightarrow \infty)t_{\mathrm{p}}]\rangle / \langle \cos^2[\omega_{\mathrm{Q}}(0)t_{\mathrm{p}}]\rangle$.

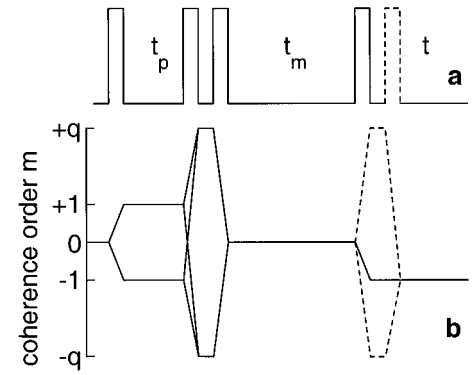

FIG. 6. (a) Pulse sequence and (b) coherence transfer pathway diagram for the "maximum coherence experiments" yielding the signals given in Table 3 for several spins I. In keeping with the standard convention the coherence path terminates at the coherence level $m = -1$. The solid pathway corresponds to the four-pulse experiment. The five-pulse sequence allows one to implement an additional $|q| = 2I$ quantum filter (cf. the dashed lines). The latter is useful for an elimination of lower rank longitudinal order that will be induced during long mixing times via quadrupolar relaxation effects.

3.3. Stimulated Echoes Using Higher Multipolar Order

Above we have mentioned how to create pure quadrupolar order from Zeeman order. Let us now discuss the generation of pure octupolar order, again for arbitrary pulse lengths. According to the (solid) coherence pathway shown in Fig. 6 (with $|q| = 3$) it involves the creation of an intermediate TQC. Since we start from a tensor of rank 1, only a SQC can be encoded during t_{p}. With the total signal written as $C_2(t_{\mathrm{p}}, t_{\mathrm{m}}, t) \equiv -s'_{1\rightarrow 3}s_{3\rightarrow \mathrm{det}}$ from Table 2 one obtains as the amplitude modulated y magnetization M_y (i.e., $M_y \propto I_y$),

$$C_2(t_{\mathrm{p}}, t_{\mathrm{m}}, t) = \tfrac{9}{20}\sin\beta_1\sin^2\beta_2\sin^3\beta_3\sin\beta_4(4 - 5\sin^2\beta_4) \times \sin^2[\omega_{\mathrm{Q}}(0)t_{\mathrm{p}}/2]\sin^2[\omega_{\mathrm{Q}}(t_{\mathrm{m}})t/2]. \qquad [7]$$

For optimum flip angles ($\beta_1 = \beta_2 = \beta_3 = 90°$ and $\beta_4 = \arccos\sqrt{\frac{11}{15}} \approx 31.1°$) this yields $C_2 = \frac{4}{5}\sqrt{\frac{3}{5}}\sin^2[\omega_{\mathrm{Q}}(0)t_{\mathrm{p}}/2]\sin^2[\omega_{\mathrm{Q}}(t_{\mathrm{m}})t/2]$. The purging time, t_{s}, should be as short as possible to avoid signal loss due to the relaxation of the TQC. Apart from this consideration the length of t_{s} is irrelevant since $T_{3\pm 3}$ is not subject to quadrupolar modulation. It is also noted that the phase of the second pulse is not important, i.e., shifting it by $\pm 90°$ gives only a smaller maximum amplitude (for $\beta_2 = \arccos\sqrt{\frac{1}{3}} \approx 54.7°$ a factor of $\frac{3}{2}\sqrt{3} \approx 2.6$ less).

In the presence of longitudinal relaxation which can lead to unwanted T_{10} contributions it will be advantageous to employ

TABLE 3
Some Simple Time Domain Signals Accessible for Several $I \geq 1$

I	Modulation of detectable signal
1	$\sin^1[\omega_Q(0)t_p]\sin^1[\omega_Q(t_m)t]$
3/2	$\sin^2[\omega_Q(0)t_p/2]\sin^2[\omega_Q(t_m)t/2]$
2	$\sin^3[\omega_Q(0)t_p]\sin^3[\omega_Q(t_m)t]$
5/2	$\sin^4[\omega_Q(0)t_p/2]\sin^4[\omega_Q(t_m)t/2]$

an additional TQ filter (cf. the dashed lines in Fig. 6) yielding $C'_2(t_p, t_m, t) \equiv s'_{1\to3}s'_{3\to det}$. For ideal flip angles (all set to 90°) this gives $(15/16)^{3/2} \approx 91\%$ of $C_2(t_p, t_m, t)$. If one deals with powders it is convenient to rewrite $C'_2(t_p, t_m, t)$ for $t = t_p$ and optimum flip angles as

$$\langle C'_2(t_p, t_m, t_p)\rangle = (\tfrac{3}{8})^2\{\zeta + \langle\cos[\omega_Q(0)t_p]\cos[\omega_Q(t_m)t_p]\rangle\}. \quad [8]$$

Here $\zeta = \sum_i w_i\zeta_i(t_p\delta_i, \eta_i)$ is an oscillatory function of t_p, but it is independent of t_m. Thus ζ may be treated as a constant when considering echo signals recorded for a fixed evolution time. For large t_p one has $\zeta \to 1$ since the coefficients $\zeta_i(t_p\delta_i, \eta_i) = 1 - 2\langle\cos[\omega_Q(\theta, \phi)t_p]\rangle$ approach unity. The latter is seen from the identity $\langle\cos[\omega_Q(\theta, \phi)t_p]\rangle = \langle\cos^2[\omega_Q(\theta, \phi)t_p/2]\rangle - \langle\sin^2[\omega_Q(\theta, \phi)t_p/2]\rangle$ and the relations given above (e.g., Eq. [5]). Hence, with an appropriate baseline subtraction a cos–cos echo function becomes accessible which is complementary to the sin–sin two-time correlation function based on Eq. [4].

The time domain signals discussed so far demonstrate that both quadrupolar *and* octupolar order are relevant in the context of stimulated echo spectroscopy. Therefore, it may be asked whether even higher multipolar spin order could be useful. For the generation of a polarization state of rank l (>3) nuclei with spin $I = l/2$ (or larger) are required. 2^l-Polar order can be generated via the coherence pathway sketched in Fig. 6 employing the states of maximum MQC ($|q| = 2I$). Then, after a sufficiently long mixing time, reconversion into detectable magnetization can be achieved via a single pulse. However, for spins $I > 1$ an additional MQ filter should be beneficial for the suppression of unwanted (lower rank) longitudinal order which can occur during the mixing time, t_m. For $I = 1$ the cycle just specified represents a more complicated but otherwise equivalent version of the sin–sin experiment with a somewhat smaller yield.

The quadrupolar modulations, $\propto s'_{1\to2I}s'_{2I\to det}$, as given in Table 3 for $1 \leq I \leq 5/2$, in principle can be monitored via stimulated echoes. The time domain signals presented there for $I > 1$ may be viewed as generalizations of those accessible via the Jeener–Broekaert experiment in the sense that now also sinusoidal modulations show up, however, taken to the power of $2I - 1$. The use of these functions may admittedly be somewhat limited because (i) no stable $I = 2$ nuclear probes are known and (ii) for $I = 5/2$ nuclei few *solid-state* NMR spectra exhibit first-order quadrupolar broadening (*24*). However, it should be noted that the application of the Jeener–Broekaert sequence to $I = 5/2$ nuclei in *liquid-like* environments was demonstrated recently (*40*).

4. FOUR-TIME CORRELATION FUNCTIONS

4.1. Successive Quadrupolar Encodings

In this type of echo experiment one correlates the NMR frequencies, in this section for brevity and analogous to Ref. (*37*) written as ω_i, at four points in time (*1*). This requires three mixing times (denoted t_{m1}, t_{m2}, and t_{m3}) and four evolution times or, stated differently, three modulation modules plus a detection pulse as schematically depicted in Fig. 1. Since here we focus on echo signals we will set $t = t_p$ throughout this section. Phase lists for generating four-time signals of the form

$$E_4(t_p, t_{m1}, t_{m2}, t_{m3}) = B\,\sin(\omega_1t_p)\sin(\omega_2t_p) \times \sin(\omega_3t_p)\sin(\omega_4t_p) \quad [9]$$

or those with some or all of the sine functions replaced by cosine functions were given elsewhere for spin-1/2 and spin-1 nuclei (*37, 43, 44*). The factor B depends on the pulse lengths and the coherence pathways chosen in a particular implementation. In an experimental study of the dynamic heterogeneity of a deuterated supercooled liquid the short t_p limit of Eq. [9], i.e., a correlation function of the type $\langle\omega_1\omega_2\omega_3\omega_4\rangle$, was explored as well (*45*).

For $I = 3/2$ nuclei it is also possible to access E_4. From Table 1 we have inferred above that sine modulations are obtained for $\Delta l = 1$ only. Consequently, to accomplish the succession of modulations as shown in Eq. [9] we need to choose coherence pathways such that during t_{m1} and t_{m3} even rank (i.e., quadrupolar) ordered and during t_{m2} odd rank (i.e., either Zeeman or octupolar) ordered states carry the desired quadrupolar modulations. Possible combinations of partial coherence pathways may be summarized as $s_{1\to2}d_{2\to3}d_{3\to2}s_{2\to det}$ and $s_{1\to2}s'_{2\to3}s'_{3\to2}s_{2\to det}$.

If T_{20} is preferred as the carrier during t_{m2}, as well, then with $s_{12}s_{22}s_{22}s_{2\to det}$ the echo signal is seen to be of the form $\sin(\omega_1t_p)\cos(\omega_2t_p)\cos(\omega_3t_p)\sin(\omega_4t_p)$, cf. Table 2. This and other combinations of quadrupolar modulation factors such as, e.g., $[1 - \cos(\omega_1t_p)]\cos(\omega_2t_p)\cos(\omega_3t_p)[1 - \cos(\omega_4t_p)]$ (which *cannot* be converted into a simple expression via a baseline correction) will, however, not be considered further in the present article. The reason is that when monitoring motional processes the *same* kind of information is encoded in each of these functions.

For $I = 3/2$, Eq. [9] represents the only four-time signal with the same type of simple encoding during each evolution

time. We have already described how to generate quadrupolar order from initial T_{10} and how to reconvert from T_{20} finally into detectable signal. However, if T_{30} is chosen as the carrier during t_{m2}, additional building blocks are needed for converting quadrupolar order and octupolar order into one another. These are presented in Table 2. In order to be able to assess the transfer amplitudes not only for the four-time correlation E_4, cf. Eq. [9], but also for several other conceivable multiple time correlation functions, we included a number of additional coefficients for SQ and DQ encoding.

Some of the transfer amplitudes put in brackets in Figs. 2, 3, and 4 are not given in Table 2, since their use may be restricted as briefly discussed here: The coefficient $s_{3\to2} = -\frac{3}{8}\sqrt{\frac{3}{5}}\sin\beta_1(4 - 5\sin^2\beta_1)\sin 2\beta_2\sin(\omega_Q t_p)$ can only be used if prior TQ filtration is not required. For optimum angles it is a factor of $\frac{5}{8}\sqrt{5} \approx 1.4$ smaller than $d_{3\to2}$ but only 10% larger than $s'_{3\to2}$. Likewise the application of (redundant) TQ filtration in conjunction with DQ encoding, for amplitudes such as $d'_{2\to3} = +\sqrt{15}/8\sin^2\beta_1\sin 2\beta_2\sin^3\beta_3\sin(\omega_Q t_p)$, reduces the maximum transfer, here by $8/3\sqrt{3}$, i.e., $d_{2\to3} \approx 1.5d'_{2\to3}$. Another coefficient not given in Table 2 is the double TQ filtered amplitude $s''_{3\to3} = +3\sqrt{3}/64\sin\beta_1(4 - 5\sin^2\beta_1)\sin^2\beta_2\sin^3\beta_3\sin[3 + 2\cos(\omega_Q t_p)]$ (cf. Fig. 4c) which, due to its complicated quadrupolar modulation and the relatively large phase cycle required to isolate it, may be not particularly useful.

4.2. Discussion of Implementations

As mentioned above an odd order polarization (either T_{10} or T_{30}) is required during t_{m2} in order to obtain a modulation as expressed in Eq. [9]. It is relatively simple to work with T_{30}, i.e., to eliminate contaminations originating from spurious Zeeman order, cf. Section 2.3. There, we have also seen that it is difficult to suppress octupolar order while retaining modulated Zeeman order unless pulse lengths can be set accurately. Since in a laboratory experiment one will usually only be able to set flip angles to *approximately* 63.4°, additional measures have to be sought: One way of suppressing unwanted longitudinal contributions exploits that under RF pulses T_{l0} varies like the lth Legendre polynomial of the flip angle. With $P_3(\cos\beta) = \frac{1}{2}(5\cos^3\beta - 3\cos\beta)$ it is seen that $\beta = \arccos\sqrt{\frac{3}{5}} \approx 39.2°$ eliminates T_{30} while retaining $\sqrt{\frac{3}{5}} \approx 77\%$ of the modulated Zeeman order. The application of one (or more) appropriately phase-cycled 39.2° pulses inserted near the end of a mixing period should thus lead to an approximate suppression of octupolar order. In any case it will be advisable to check the adjustment of the 39.2 and 63.4° pulses. This may be facilitated by utilizing a TQ filter, cf. the path associated with $s'_{3\to det}$. When applied to a potential mixture of T_{10} and T_{30} no signal will be detectable if initially only Zeeman order was present.

Now, several implementations of the sin–sin–sin–sin experiment are obvious, depending on whether T_{10} or T_{30} is chosen as carrier during t_{m2} and on whether SQ or DQ encoding is preferred during the second and third evolution times. From Table 2 the maximum total transfer amplitude for the four-time echo is given by $s_{1\to2}d_{2\to3}d_{3\to2}s_{2\to det}$ with $B_{max} = \frac{3}{16} \approx 0.19$. This amounts to about 40% of the maximum sin–sin echo amplitude, cf. Eq. [4]. Use of alternative combinations of transfer amplitudes (such as, e.g., $s_{1\to2}s'_{2\to3}s'_{3\to2}s_{2\to det}$) may reduce the signal by another factor of 2. However, in laboratory experiments not only the maximum transfer amplitudes but also the (different) dephasing times of the SQCs and the DQCs need to be taken into account.

Previous experience shows that it is highly desirable to maximize the coherence transfer particularly in the four-time stimulated echo experiments. In this context it is worthwhile to mention that advanced excitation schemes have been devised recently (*46*). These allow one to maximize the transfer amplitudes up to Sørensen's "universal bound" (*47*) if specific lengths are chosen for various evolution times. A corresponding optimization is, however, not obvious in the measurement of multiple-time correlation functions, where the evolution times need to be kept as experimentally adjustable parameters.

5. SUMMARY

In this article we have discussed theoretical aspects of the stimulated echo spectroscopy in solids and solid-like materials. We focused on nonselectively excitable spin-3/2 systems evolving under the secular first-order quadrupole Hamiltonian. A compact notation for complex phase cycles was presented. Apart from the generation of pure multipolar nuclear spin order, we have dealt with the conditions that maximize the overall amplitudes of various quadrupole modulated time domain signals. Powders were given specific consideration. In particular some conditions necessary for generating sin–sin, cos–cos, and sin–sin–sin–sin functions were described. These functions, recorded for nuclei with spin $I \leq 1$, are in widespread use for the investigation of organic substances since they allow one to obtain information which in many cases is not accessible via other experimental methods. It may be expected that with higher spins as probes these functions will find more applications in studies of the dynamics, predominantly of inorganic solids and solid-like materials.

ACKNOWLEDGMENTS

The author is indebted to G. Diezemann and A. Titze for many fruitful discussions. Stimulating conversations with B. Geil, G. Hinze, T. Jörg, F. Qi, H. Sillescu, and S. Wimperis as well as helpful comments by an anonymous referee are also gratefully acknowledged. The Deutsche Forschungsgemeinschaft is thanked for supporting this project (Grant Bo1301/5).

REFERENCES

1. K. Schmidt-Rohr and H. W. Spiess, "Multidimensional Solid-State NMR and Polymers," Academic Press, London, 1994.
2. e.g., H. Eckert, *Prog. NMR Spectrosc.* **24,** 159 (1992).

3. P. J. Bray, S. J. Gravina, D. H. Hintenlang, and R. V. Mulkern, *Magn. Reson. Rev.* **13,** 263 (1988).
4. D. Brinkmann, *Prog. NMR Spectrosc.* **24,** 527 (1992).
5. R. Blinc, J. Dolinsek, T. Apih, W. Schranz, A. Fuith, and H. Warhanek, *Solid State Commun.* **93,** 609 (1995).
6. X.-P. Tang, R. Busch, W. L. Johnson, and Y. Wu, *Phys. Rev. Lett.* **81,** 5358 (1998).
7. R. Böhmer, T. Jörg, F. Qi, and A. Titze, *Chem. Phys. Lett.* **316,** 417 (2000).
8. G. Jaccard, S. Wimperis, and G. Bodenhausen, *J. Chem. Phys.* **85,** 6282 (1986).
9. I. Furó and B. Halle, *Mol. Phys.* **76,** 1169 (1992).
10. U. Eliav and G. Navon, *J. Magn. Reson. A* **115,** 241 (1995).
11. R. Kemp-Harper, S. P. Brown, C. E. Hughes, P. Styles, and S. Wimperis, *Prog. NMR Spectrosc.* **30,** 157 (1997).
12. K. Schmidt-Rohr and H. W. Spiess, *Phys. Rev. Lett.* **66,** 3020 (1991).
13. R. Böhmer, R. V. Chamberlin, G. Diezemann, B. Geil, A. Heuer, G. Hinze, S. C. Kuebler, R. Richert, B. Schiener, H. Sillescu, H. W. Spiess, U. Tracht, and M. Wilhelm, *J. Non-Cryst. Solids* **235–237,** 1 (1998).
14. R. Böhmer, *Curr. Opin. Solid State Mater. Sci.* **3,** 378 (1998).
15. R. Böhmer, G. Diezemann, G. Hinze, and H. Sillescu, *J. Chem. Phys.* **108,** 890 (1998).
16. D. Schaefer, J. Leisen, and H. W. Spiess, *J. Magn. Reson. A* **115,** 60 (1995).
17. S. C. Kuebler, A. Heuer, and H. W. Spiess, *Macromolecules* **29,** 7089 (1996).
18. K. Funke and R. Hoppe, *Solid State Ionics* **40/41,** 200 (1990).
19. J. C. Dyre, *J. Non-Cryst. Solids* **135,** 219 (1991); J. C. Dyre and T. B. Schrøder, *Rev. Mod. Phys.* **72,** 873 (2000).
20. R. Bertermann and W. Müller-Warmuth, *Z. Naturforsch.* **53a,** 863 (1998).
21. P. Panissod, D. Aliaga Guerra, A. Amamou, J. Durand, W. L. Johnson, W. L. Carter, and S. J. Poon, *Phys. Rev. Lett.* **44,** 1465 (1980).
22. Z. Xu and J. F. Stebbins, *Science* **270,** 1332 (1995).
23. G. D. Bowden and W. D. Hutchison, *J. Magn. Reson.* **67,** 403 (1986).
24. D. Freude and J. Haase, *in* "NMR—Basic Principles and Progress" (P. Diehl, E. Fluck, H. Günther, R. Kosfeld, and J. Seelig, Eds.), Vol. 29, pp. 1–90, Springer, Berlin, 1993.
25. N. Müller, G. Bodenhausen, and R. R. Ernst, *J. Magn. Reson.* **75,** 297 (1987).
26. B. C. Sanctuary, T. K. Halstead, and P. A. Osment, *Mol. Phys.* **49,** 753 (1983); for a review see also B. C. Sanctuary and T. K. Halstead, *Adv. Magn. Opt. Reson.* **15,** 79 (1990).
27. A. Wokaun and R. R. Ernst, *J. Chem. Phys.* **67,** 1752 (1977).
28. S. Vega, *J. Chem. Phys.* **68,** 5518 (1978).
29. L. Pandey, S. Towta, and D. G. Hughes, *J. Chem. Phys.* **85,** 6923 (1986).
30. X.-P. Tang and Y. Wu, *J. Magn. Reson.* **133,** 155 (1998).
31. J. R. C. van der Maarel, *Chem. Phys. Lett.* **155,** 288 (1989).
32. M. E. Rose, "Elementary Theory of Angular Momentum," Wiley, New York, 1957.
33. R. R. Ernst, G. Bodenhausen, and A. Wokaun, "Principles of Nuclear Magnetic Resonance in One and Two Dimensions," Clarendon, Oxford, 1987.
34. G. D. Bowden, W. D. Hutchison, and J. Khachan, *J. Magn. Reson.* **67,** 415 (1986).
35. G. Bodenhausen, H. Kogler, and R. R. Ernst, *J. Magn. Reson.* **58,** 370 (1984).
36. P. J. Hore, J. A. Jones, and S. Wimperis, "NMR: The Toolkit," Oxford Univ. Press, Oxford (2000).
37. G. Hinze, R. Böhmer, G. Diezemann, and H. Sillescu, *J. Magn. Reson.* **131,** 218 (1998).
38. J. Ollerenshaw and R. E. D. McClung, *J. Magn. Reson.* **143,** 255 (2000).
39. J. Jeener and P. Broekaert, *Phys. Rev.* **157,** 232 (1967).
40. B. Wickstead, S. M. Grieve, and S. Wimperis, *Biophys. Chem.* **73,** 129 (1998).
41. F. Fujara, S. Wefing, and H. W. Spiess, *J. Chem. Phys.* **84,** 4579 (1986).
42. R. Böhmer and G. Hinze, *J. Chem. Phys.* **109,** 241 (1998).
43. S. C. Kuebler, A. Heuer, and H. W. Spiess, *Phys. Rev. E* **56,** 741 (1997).
44. U. Tracht, Dissertation, Universität Mainz, 1998; U. Tracht, M. Wilhelm, A. Heuer, and H. W. Spiess, *J. Magn. Reson.* **140,** 460 (1999).
45. G. Hinze, G. Diezemann, and H. Sillescu, *Europhys. Lett.* **44,** 565 (1998).
46. C. E. Hughes, R. Kemp-Harper, and S. Wimperis, *J. Chem. Phys.* **108,** 876 (1998).
47. O. W. Sørensen, *J. Magn. Reson.* **86,** 435 (1990).